

Mutation of the Zebrafish *glass onion* Locus Causes Early Cell-Nonautonomous Loss of Neuroepithelial Integrity Followed by Severe Neuronal Patterning Defects in the Retina

Zac Pujic and Jarema Malicki¹

Department of Ophthalmology, Harvard Medical School,
243 Charles Street, Boston, Massachusetts 02114

Mutation of the *glass onion* locus causes drastic neuronal patterning defects in the zebrafish retina and brain. The precise stratified appearance of the wild-type retina is absent in the mutants. The *glass onion* phenotype is first visible shortly after the formation of optic primordia and is characterized by the rounding of cells and disruption of the ventricular surface in the eye and brain neuroepithelia. With exception of the dorsal- and ventral-most regions of the brain, neuroepithelial cells lose their integrity and begin to distribute ectopically. At later stages, the laminar patterning of retinal neurons is severely disrupted. Despite the lack of lamination, individual retinal cell classes differentiate in the *glass onion* retina. Mosaic analysis reveals that the *glass onion* mutation acts cell nonautonomously within the retina and brain, as neuroepithelial cell morphology and polarity in these tissues are normal when mutant cells develop in wild-type hosts. We conclude that the *glass onion* mutation affects cell–cell signaling event(s) involved in the maintenance of the neuroepithelial cell layer shortly after its formation. The disruption of neuroepithelial integrity may be the cause of the neuronal patterning defects following neurogenesis. In addition, the expression of the *glass onion* phenotype in a subset of neuroepithelial cells as well as its onset following the initial formation of the neuroepithelial sheets indicate the presence of genetically distinct temporal and spatial subdivisions in the development of this histologically uniform tissue. © 2001 Academic Press

Key Words: eye; mutant; *glo*; patterning; neuroepithelium.

INTRODUCTION

Neurons in the vertebrate retina are organized with exquisite precision into three major cellular laminae: the photoreceptor cell layer (also referred to as the outer nuclear layer), the inner nuclear layer, and the ganglion cell layer. These laminae are separated by two plexiform layers consisting of neuronal projections. The inner nuclear layer is further composed of the amacrine, interplexiform, bipolar, and horizontal cells (Cajal, 1893; Rodieck, 1973; Dowling, 1987). These six neuronal cell classes, and one glial, the Muller glia, display remarkable conservation throughout vertebrate evolution. Structurally and functionally, retinæ in vertebrates as diverse as teleosts and humans are strikingly similar.

The development of the vertebrate eye and the zebrafish

eye in particular has been characterized in considerable detail (Cajal, 1893; Rodieck, 1973; Dowling, 1987; Schmitt and Dowling, 1994). The zebrafish optic primordia originate as lateral outpocketings of the anterior neural tube. By 24 hpf, through a series of morphological transformations, they assume concave shape and are called optic cups. The inner layer of the optic cups consists of a mitotically active columnar pseudostratified neuroepithelium and will give rise to cells of the retina. In the course of neurogenesis, neuroepithelial cells exit the cell cycle and differentiate into neurons and glia. Retinal neurons become postmitotic in an ordered spatiotemporal fashion. Between 27 and 28 hpf, the first postmitotic cells appear in a small ventral region of the optic cup and then progressively in the nasal, dorsal, and, finally, temporal retina. The first cells to exit the cell cycle differentiate into ganglion cells and form the innermost layer of the retina—the ganglion cell layer (Nawrocki, 1985; Hu and Easter, 1999). The remaining two major layers of the retina differentiate subsequently. The

¹ To whom correspondence should be addressed. Fax: (617) 573-4290. E-mail: jarema_malicki@meei.harvard.edu.

first postmitotic cells in the inner nuclear layer appear approximately 10 h later, also in the ventral portion of the retina. Finally, by 48 hpf, the first cells of the outer nuclear layer exit the cell cycle. As evidenced by behavioral experiments, the zebrafish retina becomes functional between 2.5 and 3.5 days postfertilization (dpf) (Easter and Nicola, 1996).

Throughout the early development of the retinal primordium, neuroepithelial cells possess polarity which is apparent in the asymmetric deployment of cellular components within the cell and on the cell surface. Cell polarization is crucial for morphogenesis, cell motility, and axonal guidance (Aaku-Saraste *et al.*, 1997; Chenn *et al.*, 1998; Andersen and Bi, 2000). In mutant animals, changes in epithelial cell polarity are frequently linked to a disruption of epithelial integrity (Muller and Wieschaus, 1996; Bilder and Perrimon, 2000). Polarity in retinal neuroepithelial cells is characterized by the presence of several cellular components at the ventricular pole (Chenn *et al.*, 1998). For example, mitotic spindles, centrosomes, and cilia are all confined to the ventricular pole until the exit of the neuroepithelial cell from the cell cycle. Junctional complexes such as adherens junctions are also located only in this region of the cell. Is the maintenance of retinal neuroepithelial cell polarity important for mechanisms such as neuronal patterning? Zebrafish mutants which affect both epithelial polarity and neuronal patterning in the retina may provide answers to this question.

In several strains of mutant zebrafish, neuroepithelial polarity defects are followed by severe disorganization of the retina. This is true, for example, for the mutants *glass onion* (*glo*), *oko meduzy* (*ome*), *nagie oko* (*nok*), and *mosaic eyes* (*moe*) (Malicki *et al.*, 1996; Jensen *et al.*, 2001). In *ome* mutant embryos, at least seven retinal cell types differentiate, but the precise stratified appearance of the retina is absent. Cell-cell interactions are sufficient to rescue the phenotype of the *ome* retinal neuroepithelial cells in genetically mosaic animals (Malicki and Driever, 1999). Complementary studies in the mouse using targeted gene knockouts have been useful in isolating genes with possible roles in retinal lamination. Gene knockouts of the NCAM, HES-1, MARCKS, and $\alpha 6$ integrin loci do lead to lamination defects however, the phenotypes are less severe than those found in *glo*, *ome*, or *nok* (Tomasiewicz *et al.*, 1993; Stumpo *et al.*, 1995; Tomita *et al.*, 1996; Georges-Labouesse *et al.*, 1998). Defects in the retinal neuroepithelium have not been reported in the mouse mutants. The extreme severity of defects in zebrafish neuronal patterning mutants suggests that the affected genes regulate mechanisms fundamental to the assembly of the retina. Characterization of these phenotypes and attempts to isolate the affected genes will provide a valuable contribution to the understanding of the genetic basis of neuroepithelial development and its relation to neuronal patterning in the CNS.

In this work, we present an analysis of neuroepithelial and neuronal patterning defects in the zebrafish mutant *glass onion*. The development of the retinal neuroepithelial sheet is disrupted in this mutant shortly after the formation

of the optic primordia. At later stages of development, *glo* displays severe defects of retinal lamination. Despite the early loss of neuroepithelial integrity and later neuronal patterning defects, the majority of retinal cell classes assayed for are present in *glo* retinæ. Mosaic analysis revealed a cell-nonautonomous behavior of the *glass onion* phenotype, indicating that it affects cell-cell interactions of the early retinal neuroepithelial sheet.

MATERIALS AND METHODS

Strains of Zebrafish

A *glo*^{m117} allele was recovered in the course of a large-scale chemical mutagenesis screen in zebrafish (Malicki *et al.*, 1996). The *glo*^{m117} embryonic phenotype is recessive, early larval lethal, and fully penetrant. Staging of embryos was performed as described previously (Kimmel *et al.*, 1995). For phenotypic observations, living mutant and wild-type siblings were collected at appropriate time points and photographed under a dissecting microscope. Detailed observations were conducted by using a Zeiss Axioscope microscope, and images were recorded using a Zeiss Axiocam digital camera (Carl Zeiss) and Photoshop software (Adobe).

Histology

Mutant and wild-type siblings were collected at appropriate time points, fixed in 1% paraformaldehyde (w/v), 2.5% glutaraldehyde (v/v), 3% sucrose (w/v) in 60 mM phosphate buffer (pH 6.9) overnight at 4°C, washed in PBST (phosphate-buffered saline with 0.1% Tween 20) for 10 min, and dehydrated in 10-min washes with a graded ethanol series (50%, 75%, 85%, 95%, and twice in 100%). Following overnight infiltration in JB-4 resin (Polysciences), embryos were embedded according to the manufacturer's instructions. Then, 5- μ m sections were collected on Superfrost Plus slides (Fisher), stained with methylene/blue-azure II for 10 s at 65°C, and rinsed in water for 10 min (Humphrey and Pittman, 1974). Sections were then stained with basic fuchsin for 30 s, rinsed in water for 10 min, dried, and mounted in Permount (Fisher).

To detect M-phase nuclei, embryos were fixed and embedded as above. Then, 4- μ m sections were collected on microscope slides and immersed in Hoechst 33258 solution (Molecular Probes; 1 μ g/ml in PBS) for 10 min, washed in PBS for 1 h, mounted in glycerol, and viewed under UV illumination.

Apoptosis

Two methods were used to evaluate apoptotic cell death: TUNEL and staining with the vital dye, acridine orange. Thirty-six hpf embryos were dechlorinated and placed in 5 μ g/ml acridine orange (acridinium chloride hemi-zinc chloride; Sigma) in E3 medium (Haffter *et al.*, 1996) for 30 min. Embryos were then washed in E3 medium and viewed with UV illumination under an Axioscope.

Alternatively, apoptotic cell death in zebrafish embryos was detected by using the Apoptosis Detection Kit (Roche Molecular Biochemicals). Eighteen and 24 hpf embryos were fixed overnight in 4% PFA in PBS and stored in methanol at -20°C. Embryos were rehydrated with PBST and digested in 10 μ g/ml proteinase K (5 min) in PBST, refixed for 20 min in 4% PFA, and then in 2:1

ethanol:acetic acid (-20°C) for 10 min. Following incubation for 1 h in equilibration buffer (supplied by the kit manufacturer), the embryos were incubated overnight at 37°C in terminal deoxynucleotidyl transferase solution with fluorescein-conjugated-dUTP according to the manufacturer's instructions. Subsequently, embryos were washed in PBST and examined for fluorescence. Cells undergoing apoptotic cell death were visible as highly fluorescent spots. Embryos at 18 and 24 hpf were photographed as described above, and the number of apoptotic cells in retinal and forebrain tissue was counted in wild-type and mutant embryos.

Immunohistochemistry

Embryos (12–84 hpf) were fixed in 4% paraformaldehyde (pH 7.2) for 2 h at room temperature, washed in PBS, infiltrated in 30% (w/v) sucrose in PBS overnight, and embedded in TBS tissue-freezing medium (Polysciences). Then, $14\text{-}\mu\text{m}$ sections were thaw-mounted on Superfrost Plus slides (Fisher Scientific) and stored at room temperature for 1 h. Sections were rehydrated in PBS (5 min) and blocked for 1 h in 1% BSA (w/v), 10% (v/v) normal goat serum, 0.5% Triton X-100 (v/v) in PBS. The primary antibody was diluted in block solution and applied for 2 h. Sections were washed in PBST (three times, 5 min each), stained with the secondary antibody diluted 1:1000 in block solution for 1 h at room temperature, washed as previously described, and mounted in 50% glycerol (v/v), 2% *N*-propyl gallate (w/v), 200 mM Tris-HCl (pH 8.0), and viewed with a Leica TCS4D confocal microscope.

Immunohistochemistry was done by using the following antibodies and dilutions: Zpr-1 (formerly Fret 43) for red-green double cones (1:200; Oregon Monoclonal Bank); anti-carbonic anhydrase for Muller glia (1:100; gift from Paul Linser); anti-phosphorylated H3 histone for mitotic cells (1:400; Upstate Biotechnology); anti-tyrosine hydroxylase for interplexiform cells (1:100; Chemicon); anti- γ -tubulin for centrosomes (1:200; antibody from Sigma Chemical or 1:10 antibody from Pavel Draber), or Zn8 for ganglion cells (1:25; Oregon Monoclonal Antibody Bank). Anti-mouse or anti-rabbit secondary monoclonal antibodies conjugated to Cy3 or Cy5 were obtained from Jackson ImmunoResearch. Staining for γ -tubulin required the treatment of the embryos for 5 min in acetone at -20°C prior to blocking.

For F-actin staining, sections were prepared as above, washed in PBS (5 min), blocked in 1% (w/v) BSA in PBS for 1 h, incubated for 1 h in Alexa 488-conjugated phalloidin (1:40; Molecular Probes), washed with PBS (three times, 10 min each), mounted, and viewed by using confocal microscopy as above.

In Situ Hybridization

Whole-mount *in situ* hybridization was performed as described previously using digoxigenin-labeled antisense RNA probes and anti-digoxigenin alkaline phosphatase-conjugated antibodies (Boehringer Mannheim) (Oxtoby and Jowett, 1993). After hybridization, embryos were dehydrated, embedded in JB-4 resin (Polysciences) as described above for histology, and sectioned. Sections were photographed by using transmitted light microscopy. Embryos were reared in embryo medium supplemented with 0.003% 1-phenyl-2-thiourea to inhibit the development of pigmentation (Westerfield, 1994).

Mosaic Analysis

Blastomere transplantations were performed as described previously (Ho and Kane, 1990; Halpern *et al.*, 1993; Westerfield, 1994;

Malicki, 1999). Donor embryos were injected at the 2–8 cell stage with a 2.5% mixture of biotin- and Texas Red-conjugated dextrans in a 9:1 ratio (Molecular Probes). At blastula stage, 10–40 cells were removed from a labeled donor with a glass pipette and transferred to an unlabeled host. Incorporation of donor cells into the retinal neuroepithelial layer was scored at 24 h by immunofluorescence. Host embryos were cryosectioned and processed for immunofluorescence by using anti-H3 histone and anti- γ -tubulin antibodies as described above, with the additional modification that dextran tracer signal was detected by using Alexa Fluor 488-conjugated streptavidin (1:1500; Molecular Probes) during the secondary antibody step. Confocal analysis of mosaic clones was carried out as above. The number of centrosomes located more than a nuclear diameter from the ventricular surface was determined in each clone for the retina and brain of mosaic embryos.

RESULTS

The glass onion Mutant Embryos Display Abnormal Head and Eye Morphogenesis

The *glass onion* (*glo*) mutant embryos display abnormal development of the central nervous system, somites, notochord, and tail (Fig. 1). This analysis focuses primarily on the brain and the retina. The early central nervous system primordium in zebrafish is a solid rod of cells termed the neural keel and not a neural tube as in many other vertebrates. The optic primordia begin to develop at ca. 11.5 h postfertilization (hpf) as two lateral outpocketings emerging at the anterior portion of the neural keel (Figs. 1A and 2A) (Schmitt and Dowling, 1994). Their walls consist of pseudostratified neuroepithelia of mitotically active cells. The optic primordia are initially somewhat flattened so that their ventral walls are directed towards the yolk, while their dorsal walls face the surface ectoderm. Starting at ca. 14 hpf, the optic primordia rotate along their anteroposterior axes. As a result, their dorsal walls, fated to become the neural retinae, turn away from the brain, while the ventral walls, fated to become the pigmented epithelia, turn toward it (Figs. 2E and 2G). In parallel, the retina progressively detaches from the neural keel starting posteriorly so that, by 16 hpf, the optic primordia remain attached to the neural keel only at the optic stalk. During the next few hours, the optic primordia invaginate and the lens rudiments start to form from the overlying epithelium. Concomitant to this morphological transformation, cells in the initially ventral and now medial layer of the optic lobe develop the thinner and more flattened morphology of the pigmented epithelium, while cells in the dorsal (now lateral) layer retain the columnar neuroepithelial morphology. By 24 hpf, the optic primordium has invaginated forming a cup (Fig. 2I).

The *glo* mutant phenotype is first discernable at ca. 12 hpf by the disrupted development of the anterior neural keel and the optic primordia (Fig. 1B, compare with the wild type in Fig. 1A). This defect becomes progressively more obvious at later stages of development (Figs. 1D and 1F). By 20 hpf, mutant embryos are easy to distinguish from wild-type siblings due to the failure of the optic cups to detach

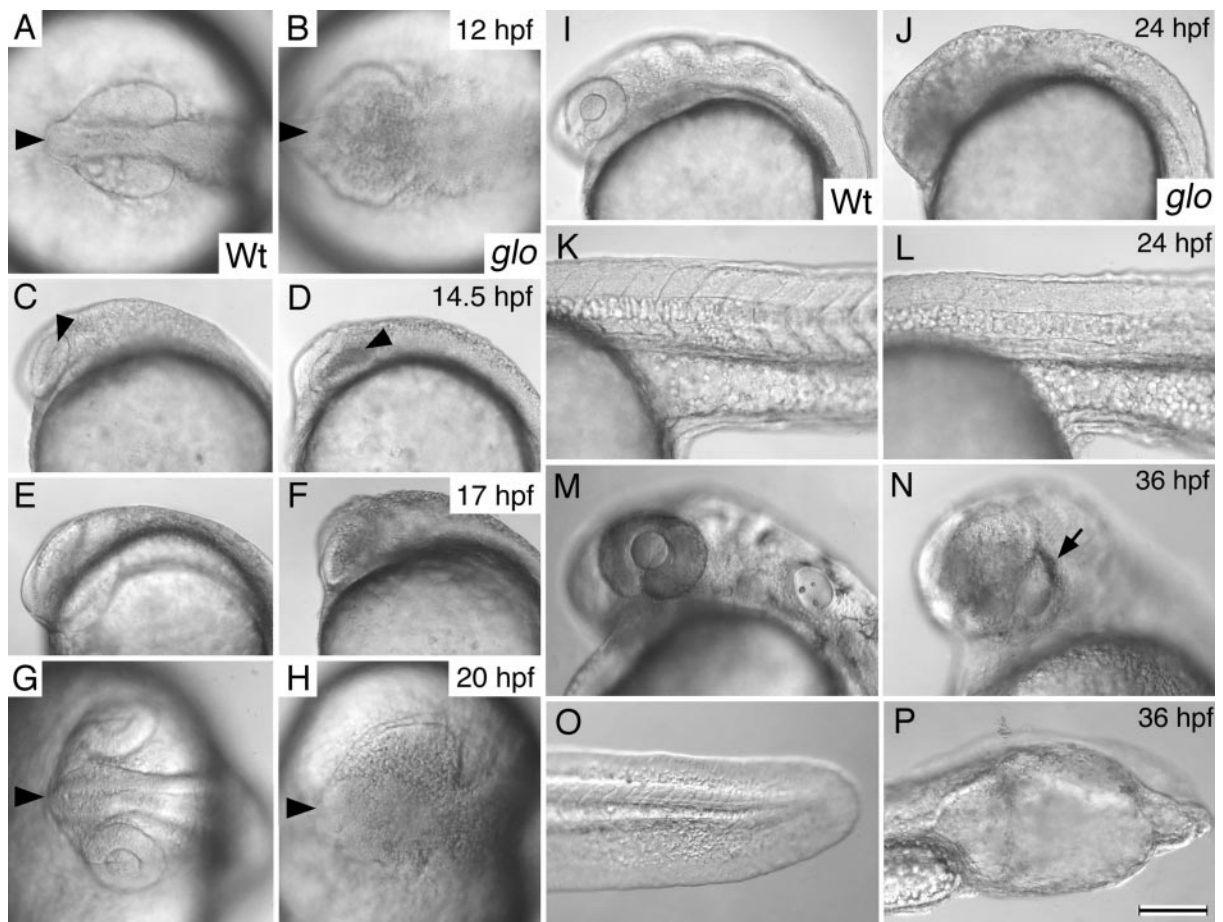


FIG. 1. The *glass onion* phenotype during embryonic development. Dorsal views are shown in (A), (B), (G), and (H). All other panels show lateral views. At 12 hpf, the eye and brain primordia in *glo* embryos (B) lack a well-delineated appearance (A). The crease in the optic primordium (arrowhead in C and D) is broader and more diffuse in *glo* embryos at 14.5 or 17 hpf (D and F, compare with the wild type in C and E). At 20 and 24 hpf, lens, retina, and brain are poorly differentiated in *glo* embryos (H, J) compared to the wild type (G, I), and the optic primordia do not detach from the neural keel. At 24 hpf, somitic boundaries are not well-defined in *glo* embryos (L) compared with the wild type (K), and the development of other structures is also disrupted. At 36 hpf, the retinal pigmented epithelium forms only in the dorsal region of the *glo* eye (arrow in N), while, in wild-type embryos, it surrounds the entire retina (M). At 36 hpf, the tail of *glo* embryos is clubbed (P) compared with the wild type (O). Scale bar equals 140 μm for (A), (B), (G), and (H); 110 μm for (K) and (L); 180 μm for (I) and (J); 140 μm for (O) and (P); 160 μm for (M) and (N); 190 μm for (C–F).

from the neural keel (Fig. 1H, compare with Fig. 1G). In mutant embryos, the lens is smaller and displaced ventrally (not shown). Although *glo* body pigmentation is normal, the eye is mostly unpigmented with the exception of its dorsal-most region (Fig. 1N, arrow indicates pigmentation in the dorsal retina, compare with Fig. 1M). Somitogenesis is also abnormal. In wild-type embryos, the first somites appear at ca. 10 hpf (Kimmel *et al.*, 1995). In *glo* mutants, at the level of gross morphology, somite formation is delayed and the somitic boundaries are less distinct (Fig. 1L, compare with Fig. 1K). The tail is shortened and club-shaped (Fig. 1P, compare with Fig. 1O).

Histological examination of the *glo* brain at successive developmental stages has revealed neuroepithelial defects

followed by abnormal neuronal patterning. In transverse sections through the embryo at 10 hpf, *glo* mutants are indistinguishable from wild-type sibling controls (data not shown). By 12 hpf, however, histological analysis demonstrates abnormal morphology of the ventricular surface in the brain and eye neuroepithelia. About this time, rounded cells, presumably originating from the neuroepithelial sheet, appear in the ventricular lumen of the optic vesicles (Fig. 2B, compare with the wild type in Fig. 2A). The number of these cells progressively increases in the course of development (arrows in Fig. 2D, compare with Fig. 2C). By 17 hpf, both eye and brain neuroepithelia undergo extensive loss of tissue integrity, leading to the absence of a ventricular surface in the retinal neuroepithelium as well as

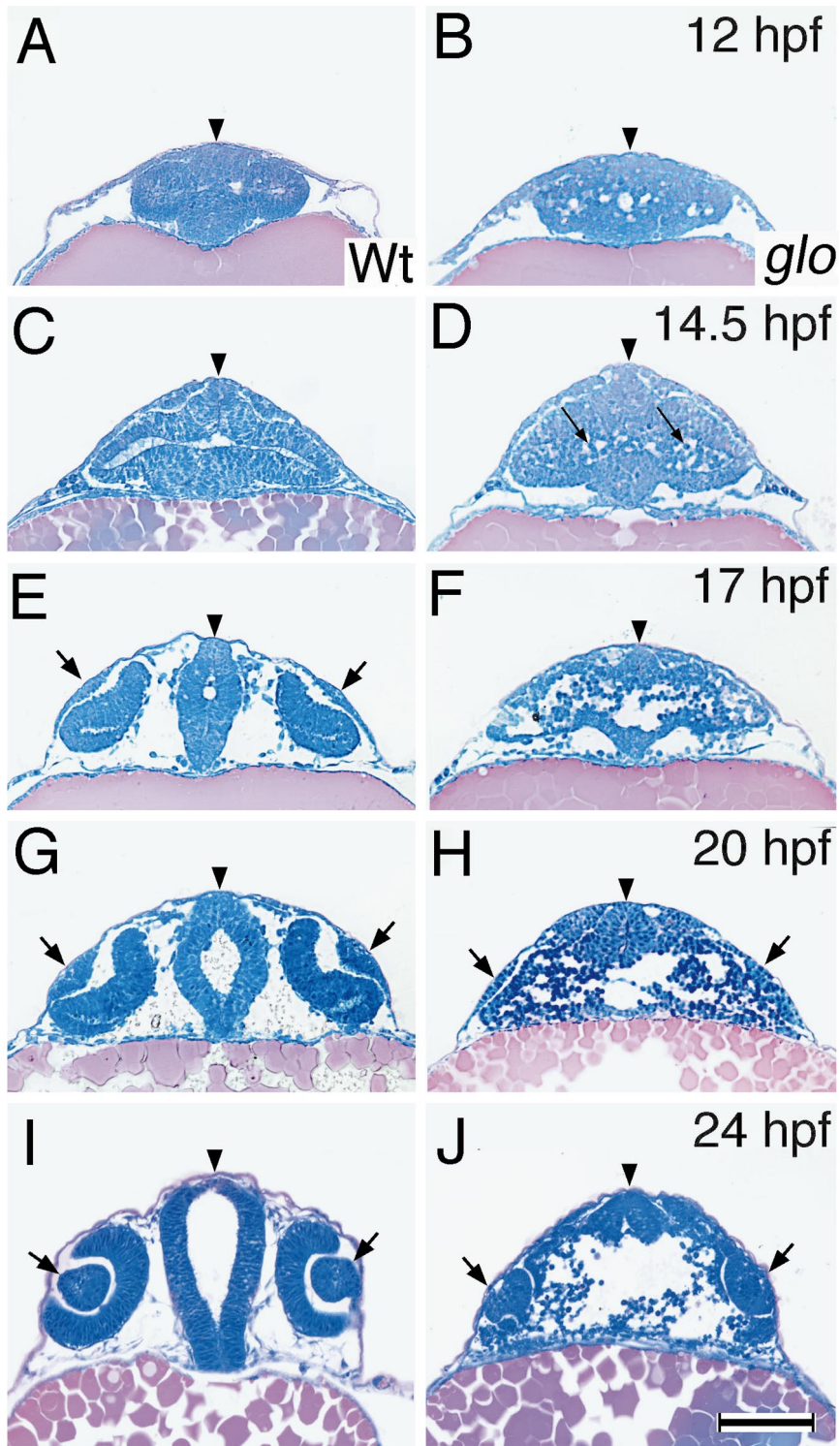


FIG. 2. Histological analysis of *glass onion* embryonic development. Transverse sections through the center of the eye and lens. At 12 hpf, the optic primordia of wild-type embryos form two lateral outpocketings of the neural keel neuroepithelium (A). By this time, the loss of neuroepithelial cell layer integrity is first visible in *glo* embryos near the ventricular surface (B). By 14.5 hpf, the loss of integrity in *glo* embryos (D) becomes more obvious throughout the neuroepithelium of the optic primordium. Arrows in (D) indicate ectopically located cells which fill the lumen of the optic vesicle (compare to the wild type in C). By 17 hpf, the optic cups in wild-type embryos detach from the neural keel and lens tissue starts to differentiate from the overlying ectoderm. In mutant embryos, the loss of neuroepithelial integrity

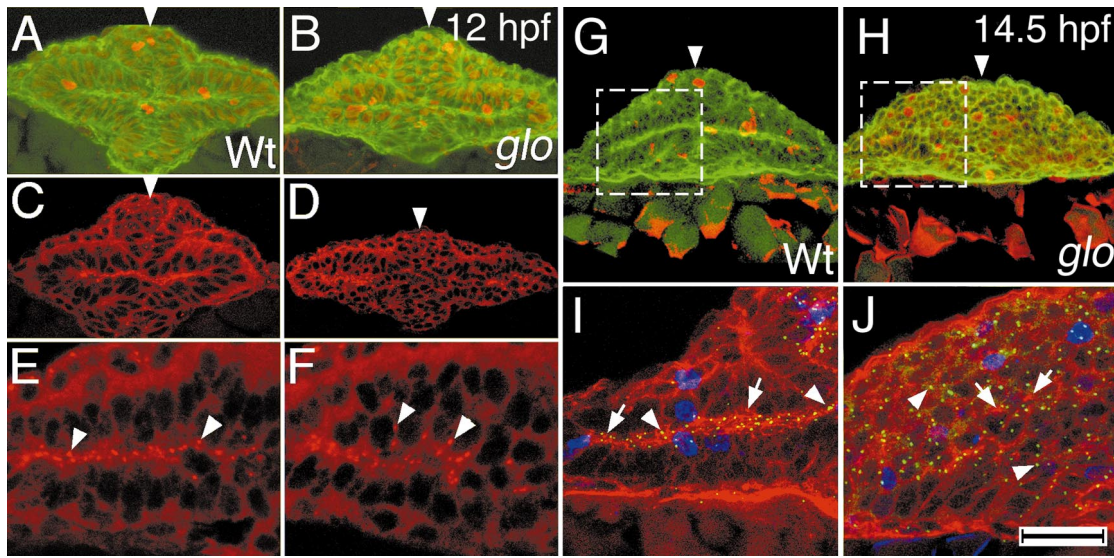


FIG. 3. Localization of ventricular markers in wild-type (Wt) and *glass onion* (*glo*) embryos at 12 and 14.5 hpf. In (A), (B), (G), and (H), actin is visualized with Alexa Fluor 488-conjugated phalloidin to show the tissue architecture (green). M-phase nuclei are visualized with an anti-phosphorylated H3 histone antibody and Cy3 or Cy5 fluorescence (red in A, B, G, and H, blue in I and J). Centrosomes are visualized by using an anti- γ -tubulin antibody and Cy3 fluorescence (red in C–F, green in I and J). In wild-type embryos, M-phase nuclei and centrosomes localize to the ventricular surface of neuroepithelial sheet in the optic primordia and neural keel (A, C, E). At 12 hpf, M-phase nuclei are not significantly displaced in *glo* embryos (B) as compared to the wild type. The *glo* centrosomes, on the other hand, appear to be somewhat more dispersed (F) than in the wild type (E). At 14.5 hpf, M-phase nuclei do not localize to the ventricular surface of the neuroepithelial sheet in *glo* embryos (H, compare with wild-type animals in G). At 14.5 hpf, in wild-type embryos, centrosomes (small green spots shown by arrowheads), adherens junction-associated actin foci (red, shown by arrows), and M-phase nuclei (blue) are localized in a narrow region at the ventricular surface of the optic lobe neuroepithelia. The few M-phase nuclei that localize away from the ventricular surface belong to the epidermis (I). In *glo* embryos, on the other hand, all three markers are mispositioned (J). Dashed boxes in (G) and (H) indicate the regions shown in (I) and (J), respectively. (I, J) and (G, H) show different specimens. Vertical arrowheads indicate the midline. Scale bar equals 70 μ m in (A–D); 30 μ m in (E) and (F); 90 μ m in (G) and (H); 35 μ m in (I) and (J).

to the absence of a continuous RPE cell layer (Fig. 2F, compare with Fig. 2E). This defect is not present in the dorsal- and ventral-most diencephalon of *glo* embryos. The neuroepithelia of these areas retain normal morphology, characterized by the presence of well defined apical and basal surfaces. However at 20 and 24 hpf, only the dorsal brain anterior to the midbrain remains unaffected (Figs. 2H and 2J). This suggests that these regions of the brain are at least in part under the control of different genetic mechanisms than the central portion of the brain and optic primordia. *glass onion* does not appear to involve a general defect in the epithelial structure because the epidermis,

spinal cord, otic vesicles, and some regions of the brain neuroepithelium are not affected by this mutation.

Histological analysis also reveals that lens formation is retarded in that the lens does not develop its typical rounded morphology and frequently remains connected to the surface epithelia at 24 hpf and beyond (Fig. 2J, compare with Fig. 2I). In addition to the early developmental defects which result in larval lethality of the homozygotes, heterozygous animals also display a dominant adult phenotype characterized by the appearance of bulges in the regions of the heart and abdomen possibly due to the presence of tumors or edema (not shown). This

continues throughout the optic cups and neural tube (F). Furthermore, optic cups have not detached from the neural tube. At 20 hpf, the lens placodes in *glo* embryos (H) are smaller compared to those of the wild type (arrows in E–J). At 24 hpf, the neuroepithelia in the eye and brain continue to display a loss of integrity in mutant embryos (J) compared with the wild type (I). Unlike other regions, the dorsal-most aspects of the brain remain normal in *glo* embryos (F, H, J). This, to a lesser extent, is also true for the ventral-most regions (F). By 24 hpf, lens tissue has detached from the overlying epidermis in wild-type embryos (I). In contrast, mutant lenses remain attached to the epidermis (J). Arrowheads indicate midline. Arrows indicate lenses. Scale bar equals 100 μ m.

phenotype is only partially penetrant and appears at variable age.

Polarity of Neuroepithelial Sheet Is Disrupted in *glass onion* Embryos

To further evaluate the nature of the neuroepithelial defect, we determined the position of markers of neuroepithelial polarity in *glass onion* embryos. Neuroepithelia of the developing neural tube show a distinct polarity evident in the apical localization of several subcellular entities such as centrosomes, adherens junctions, cilia, and mitotic nuclei (Sauer, 1935; Hinds and Ruffett, 1971; Astrom and Webster, 1991; Aaku-Saraste *et al.*, 1996, 1997; Chenn *et al.*, 1998). Disruption of neuroepithelial polarity in the optic lobe has been observed for the mutations of the *ome* locus which subsequently affect neuronal patterning in the retina (Malicki and Driever, 1999). To determine whether similar defects are present in the *glo* brain and eye neuroepithelia, we determined the localization of these markers in mutant animals at several stages of development. The positioning of centrosomes was determined with an antibody directed to γ -tubulin, a major component of this structure (Sterns, 1994). Because adherens junctions are associated with dense deposits of actin microfilaments (Geiger *et al.*, 1983; Volberg *et al.*, 1986), the presence of F-actin foci has been used as an indicator of adherens junctions. To detect F-actin microfilaments within neuroepithelial cells, we used fluorophore-conjugated phalloidin. To determine the position of dividing nuclei we used two methods: an antibody to phosphorylated-H3 histone protein and Hoechst staining. The H3 histone is highly phosphorylated during late G₂ and early M-phase and thus is a good indicator of nuclei that are undergoing mitosis (Hendzel *et al.*, 1997). Similarly, Hoechst staining allows one to visualize condensed chromatin and is another indicator of M-phase nuclei (Malicki and Driever, 1999).

The polarity of the eye and brain neuroepithelial sheets in *glo* at 12 hpf appears largely normal as indicated by the ventricular positions of centrosomes and M-phase nuclei (Figs. 3B, 3D, and 3F; compare with the wild type in Figs. 3A, 3C, and 3E). The positions of centrosomes in the mutant appear to be only slightly more dispersed than in the wild type (Fig. 3F, compare with Fig. 3E). By 14.5 hpf, however, the distribution of M-phase nuclei, centrosomes, and adherens junction-associated actin appears to be drastically different in *glo* as compared to the wild type. All three of these structures are no longer associated with the ventricular surface (Figs. 3H and 3J, compare with Figs. 3G and 3I). This phenotype persists at 18 (Figs. 4B, 4D, and 4H) and 36 hpf (Figs. 4L, 4N, and 4P). Throughout this period, although severely disorganized, the presumptive neuroepithelial cells in the brain and eye regions of the neural tube continue to divide at a normal or higher rate (Figs. 4B, 4H, and 4L). To further investigate the neuroepithelial defect, we performed staining of sections through wild-type and mutant retinæ with the DNA-binding dye Hoechst-33258,

which allows one to monitor nuclear morphology. In wild-type animals, the nuclei of eye and brain neuroepithelia are characterized by elongated shape. The M-phase nuclei, easy to distinguish by virtue of condensed chromatin, are consistently located at the ventricular surface (Figs. 4C and 4E, arrowheads in 4C indicate M-phase nuclei; Fig. 4I). In contrast to the wild type, *glo* neuroepithelial nuclei are rounded and M-phase nuclei are broadly dispersed. The boundary between the retina and brain is no longer distinct (Figs. 4D, 4F, and 4J, compare with Figs. 4C, 4E, and 4I). In the brain at 18 hpf, cell nuclei in the ventral- and dorsal-most regions retain elongated wild-type morphology. Cell nuclei of the anterior telencephalon and spinal cord also retain elongated wild-type morphology (data not shown). At 24 hpf, this pattern persists (Fig. 4J, compare with Fig. 4I) with the exception of the midbrain where some ventral regions lose correct morphology. In Hoechst-stained preparations, the otic vesicle epithelium is also intact in mutant embryos at 24 hpf (data not shown). These results show that neuroepithelial sheet polarity is disrupted in the mutant retina and brain. Since the first postmitotic cells appear at 28 hpf in the retina, the ectopic localization of markers for neuroepithelial cell polarity at 14.5 hpf indicates that the *glo* defect precedes neurogenesis by 13.5 h or more.

The Loss of Neuroepithelial Integrity Is Followed by Apoptosis

Histological inspection revealed the presence of large empty spaces in the anterior brain and the optic primordia/vesicles of mutant animals at 17 hpf and beyond, suggesting that many of the abnormally localized cells undergo cell death. To further investigate this possibility, we performed TUNEL (TdT-mediated dUTP nick-end labeling) (Gavrieli *et al.*, 1992) and acridine orange staining (Abrams *et al.*, 1993) to detect the presence of apoptotic cell bodies at several stages of development. The TUNEL method labels fragmented DNA which is characteristic of apoptotic cell death (Abrams *et al.*, 1993). Cell death in neural tissue is frequently a component of wild-type embryonic development (Oppenheim, 1985). Consistent with this observation, we have detected cell death in both wild-type and *glo* animals at 18 hpf (Figs. 5A and 5B). The levels of apoptotic cell death are indistinguishable between wild-type and mutant animals at this stage. The number of apoptotic cells in the retina and forebrain regions of wild-type and *glo* embryos at 18 hpf was 150 ± 30 ($n = 5$) and 178 ± 34 ($n = 6$), respectively. At 24 and 36 hpf, however, the level of cell death in the same region of mutant animals is markedly increased compared to the wild type (Figs. 5D and 5F, compare with Figs. 5C and 5E). At 24 hpf, the number of apoptotic cells was fairly consistent in the forebrain and eyes of wild-type animals. In contrast, the level of cell death in the mutant varied from approximately normal to several times the wild-type level (Fig. 5G). Apoptotic cells appeared to be located predominantly in the forebrain. This analysis

indicates that the loss of neuroepithelial integrity is followed by elevated cell death with a delay of up to 12 h.

glass onion Affects the Patterning of Several Postmitotic Cell Classes in the Zebrafish Retina

The *glo* locus is involved in the cellular organization of the zebrafish retina. At 3 dpf, cells in the mutant retina do not form distinct laminae or optic nerve (Malicki *et al.*, 1996). To investigate whether individual cell classes are present in the *glo* retina and where they are localized, we performed immunohistochemical staining using cell class-specific antibodies and *in situ* hybridization using cell class-specific RNA probes. We analyzed three out of the six major neuronal cell classes: ganglion cells (Figs. 6A and 6B), interplexiform cells (data not shown), and photoreceptors (Figs. 6E and 6F). Additionally, we characterized the phenotype of the Muller glia (Figs. 6C and 6D). Except for interplexiform cells, normally found in the inner nuclear layer, the cell types detected in these labeling experiments are present in *glo* but are grossly mislocalized (Figs. 6B, 6D, and 6F) compared with cells found in wild-type retinæ (Figs. 6A, 6C, and 6E). Tyrosine hydroxylase immunoreactivity is first detected in wild-type retinæ at ca. 60 hpf (Guo *et al.*, 1999). In *glo* retinæ, this marker for interplexiform cells was not expressed at least until 84 hpf. Catecholaminergic neurons expressing tyrosine hydroxylase were, however, detected at this stage in the CNS of mutant embryos (data not shown). Based on these experiments, we conclude that the majority of cell classes assayed for in the *glo* retinæ are specified but do not localize to their proper positions.

In the mutant retinæ, some of the ectopically localized cells appear to be well differentiated. We evaluated the morphology of red, green, rod, and blue opsin-expressing photoreceptor cells. In mutant retinæ, these cells are characterized by elongated morphology (Figs. 6F, 6H, 6J, and 6L). This elongated appearance is a property of differentiated photoreceptor cells in wild-type retinæ (Figs. 6E, 6G, 6I, and 6K). Furthermore, photoreceptor cells in mutant retinæ accumulate opsin mRNA in one pole of the cell, another feature of well-differentiated wild-type cells (Figs. 6H, 6J, and 6L, compare with Figs. 6G, 6I, and 6K). In wild-type retinæ, photoreceptor cells form a compact layer adjacent to the retinal pigmented epithelium (RPE). In mutant retinæ, on the other hand, photoreceptor cells form round clusters, rosettes, sometimes containing 10 cells or more in a plane of a single section with the opsin-expressing poles at the center of each rosette (Figs. 6H, 6J, and 6L). Similar to photoreceptors, ganglion cells in mutant embryos also tend to form aggregates (arrows in Fig. 6B). The axons of ectopic ganglion cells stain with the Zn8 antibody and sometimes form fascicles in abnormal locations (arrowhead in Fig. 6B). The axons of *glo* ganglion cells do not form a distinct optic nerve. The tendency of photoreceptor and ganglion cells to form homotypic aggregates indicates that they preferentially adhere to cells of the same type and that this aspect of

cell-cell interaction is not significantly impaired in *glo* embryos.

The Loss of Neuroepithelial Integrity Is Independent of the Early Patterning Events in the Optic Lobe

Several factors have been shown to regulate the early patterning of the vertebrate eye. *Sonic hedgehog*-, *Rx*-, *Six*-, and *Pax*-type genes are among the best characterized. Each of them is represented in zebrafish by two or more paralogs (Krauss *et al.*, 1993; Macdonald *et al.*, 1995; Lun and Brand, 1998; Nornes *et al.*, 1998; Seo *et al.*, 1998; Chuang *et al.*, 1999). To investigate whether the *glo* phenotype of the optic lobe neuroepithelium is caused by early optic lobe patterning defects, we analyzed the expression patterns of several genes known to be involved in embryonic patterning by *in situ* hybridization. At 12 hpf, the expression of *Zrx1*, *Zrx2*, *Zrx3*, *Pax2.1*, *Six-3*, *Six-6*, and *shh* in *glo* embryos is indistinguishable from that found in the wild type (Fig. 7, and data not shown). Although we cannot exclude the possibility that yet other early patterning genes are affected in the mutant, these results suggest that the *glo* neuroepithelial defect is independent of early patterning events in the optic lobe.

The glass onion Mutation Acts Cell-Nonautonomously to Affect Neuroepithelial Cell Phenotype

The loss of neuroepithelial integrity in *glo* may be due to either an intrinsic defect in the neuroepithelial cells or defective interactions with other cells in the retinal neuroepithelium or elsewhere. To determine which of these possibilities is true, we performed mosaic analysis of the *glo* neuroepithelial phenotype using the well-established technique of blastomere transplantations (Ho and Kane, 1990; Halpern *et al.*, 1993; Malicki and Driever, 1999). Following the transplantation of dextran-labeled blastomeres from a donor to a host embryo, a fraction of donor blastomeres contributes to the retinal neuroepithelium (Malicki and Driever, 1999). To study the *glo* neuroepithelial phenotype, host embryos containing donor-derived cells in the retinal neuroepithelium were collected at 24 hpf. To determine the phenotype of neuroepithelial cells, mosaic hosts were fixed, cryosectioned, and stained with three probes: a fluorophore-conjugated avidin to detect dextran, anti- γ -tubulin antibody to determine the position of centrosomes, and anti-phosphorylated histone antibody to determine the position of M-phase nuclei (Hendzel *et al.*, 1997). The progeny of a *glo/+* \times *glo/+* cross were used as both donors and hosts. We have focused our analysis on two types of mosaic animals: wild-type host embryos containing wild-type donor-derived clones, and wild-type host embryos containing *glo* donor-derived clones.

These experiments have shown that, as expected, wild-type donor clones in wild-type hosts always form contact

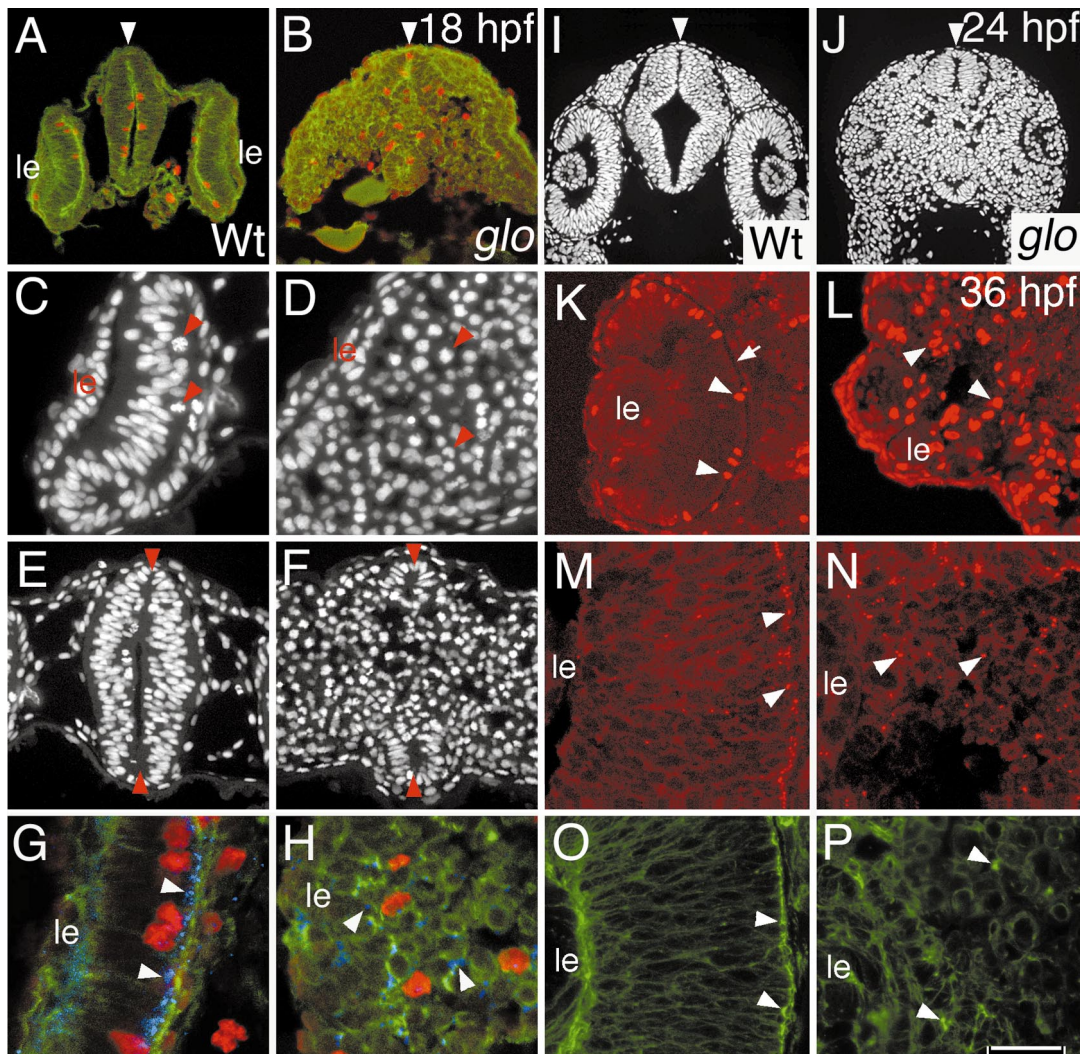
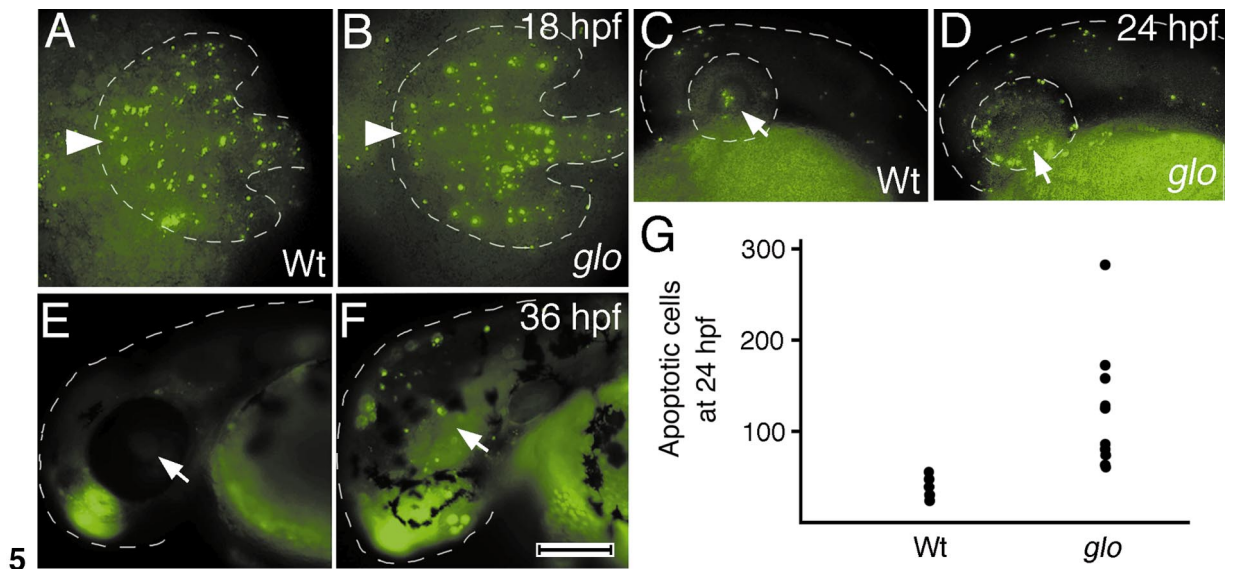
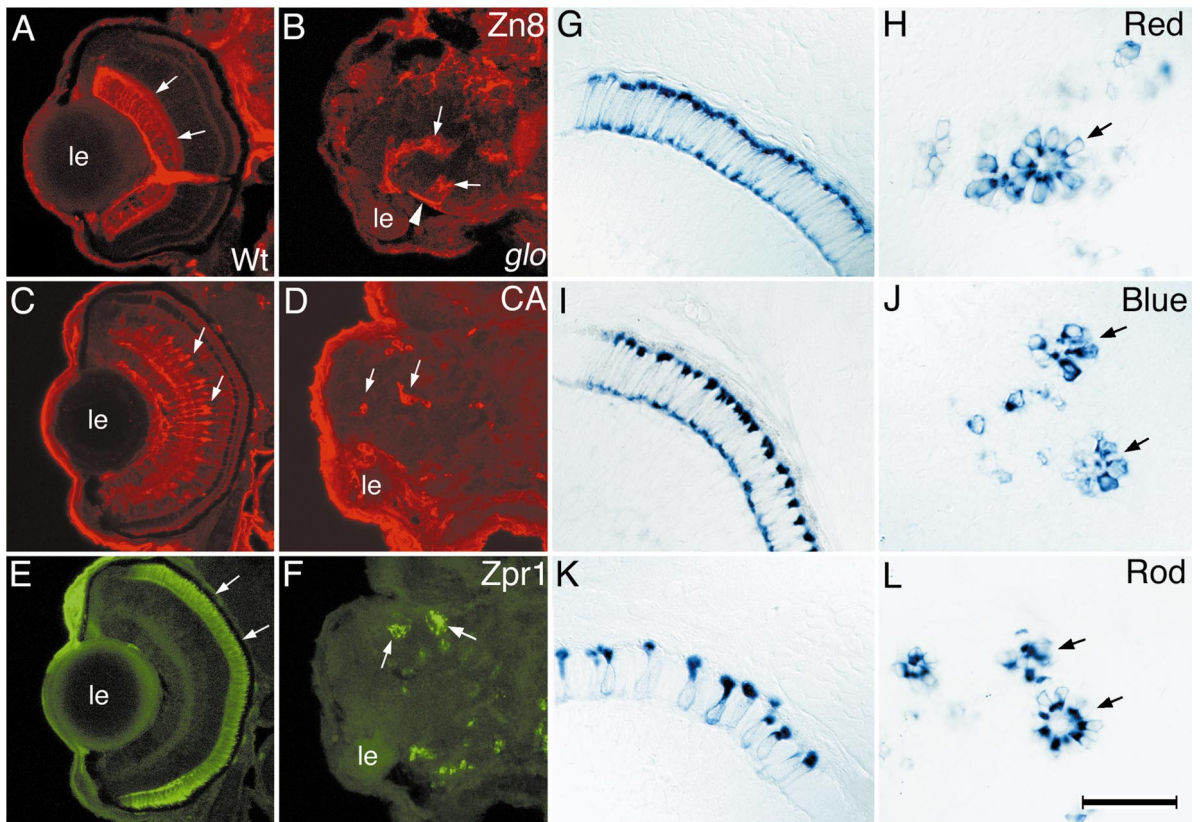


FIG. 4. Localization of ventricular markers in wild-type (Wt) and mutant (*glo*) embryos at 18 (A–H), 24 (I, J), and 36 (K–P) hpf. Adherens junction-associated actin foci are visualized with Alexa Fluor 488-conjugated phalloidin (green). M-phase nuclei are labeled with an anti-phosphorylated H3 histone primary antibody and Cy3- or Cy5-conjugated secondary antibody (red in A, B, G, H, K, L). Cell nuclei are visualized with Hoechst 33258 staining (C–F, I–J). The position of centrosomes is visualized with an anti- γ -tubulin primary antibody and Cy3- or Cy5-conjugated secondary antibody (blue in G–H, red in M and N). (A) In wild-type (Wt) embryos at 18 hpf, M-phase cell nuclei and adherens junction-associated foci localize to the ventricular surface of the neuroepithelial sheet in the optic primordia and neural keel. (B) In *glo* embryos, on the other hand, actin foci and M-phase nuclei distribute throughout the neuroepithelial tissue. In *glo* embryos, the optic primordia have not detached from the neural keel at 18 hpf. The dorsal- and ventral-most parts of the mutant neural tube retain wild-type morphology (compare B with A, arrowheads indicate the midline). (C) In wild-type embryos, the Hoechst 33258-visualized neuroepithelial nuclei are elongated and aligned along the apical–basal axis. M-phase nuclei (arrowheads) localize to the ventricular surface of the retinal neuroepithelium. (D) In *glo* embryos, cell nuclei are rounded, and mitotic nuclei are located ectopically. (E) In wild-type embryos, nuclei of the neural tube are elongated. (F) In mutant embryos, on the other hand, cell nuclei are rounded and the integrity of the neural tube is disrupted except in the dorsal- and ventral-most regions (arrowheads in E and F indicate the midline). (G) In wild-type embryos, mitotic nuclei (red), centrosomes (blue, shown with arrowheads), and adherens junction-associated F-actin foci (green) localize to the ventricular surface of neuroepithelial cells. (H) In contrast to that, in mutant embryos, these markers of the ventricular surface distribute ectopically. Note the rounded appearance of mutant cells compared to the wild type (compare H with G). (I) In wild-type embryos at 24 hpf, the lenses have detached from the overlying ectoderm. (J) In mutant embryos, the lenses are poorly developed and the optic primordia remain attached to the neural tube. The dorsal- and ventral-most regions of the neural tube are intact. (K) In wild-type embryos at 36 hpf, the retinal pigmented epithelium is developed (arrow) and M-phase nuclei localize to the ventricular surface of the neuroepithelial sheet (arrowheads). (L) In mutant retinæ, M-phase nuclei are distributed ectopically, the retinal pigmented epithelium is undetectable, and the lens is smaller. In wild-type retinæ, centrosomes (arrowheads in M) and actin foci (arrowheads in O) are positioned in a narrow zone at the ventricular surface of the neuroepithelial sheet. In contrast, mutant centrosomes (arrowheads in N) and adherens junctions (arrowheads in P) are distributed throughout the retina. Cells are elongated in wild-type retinæ (O) and rounded in mutant retinæ (P). le, lens. Scale bar equals 140 μ m in (A) and (B); 55 μ m in (C) and (D); 77 μ m in (E) and (F); 40 μ m in (G) and (H); 100 μ m in (I) and (J); 50 μ m in (K) and (L); and 20 μ m in (M–P).



5



6

FIG. 5. Apoptosis in *glo* embryos. Apoptotic cells are visualized using TUNEL (A–D) or acridine orange (E, F) staining and appear as small green spots. (A, B) Dorsal view of wild-type (Wt) and mutant (*glo*) embryos at 18 hpf. Levels of apoptosis in mutant embryo brain and optic primordia are indistinguishable from those found in the wild type. (C, D) Lateral view of embryos at 24 hpf. Apoptosis in the forebrain and retina of mutant embryos (D) is elevated compared to the wild type (C). At 36 hpf, apoptosis in mutant embryos (F) remains elevated compared to the wild type (E). (G) Counts of apoptotic cells in brains and optic primordia of 9 wild-type and 11 *glo* embryos at 24 hpf. The level of apoptosis in *glo*, although variable, consistently exceeds wild-type levels. Dashed lines outline the anterior neural tube and optic primordia in (A) and (B), head and eye in (C) and (D), and head in (E) and (F). In all panels, rostral is to the left. Arrowheads show the midline and arrows indicate the lens. Scale bar equals 150 μ m.

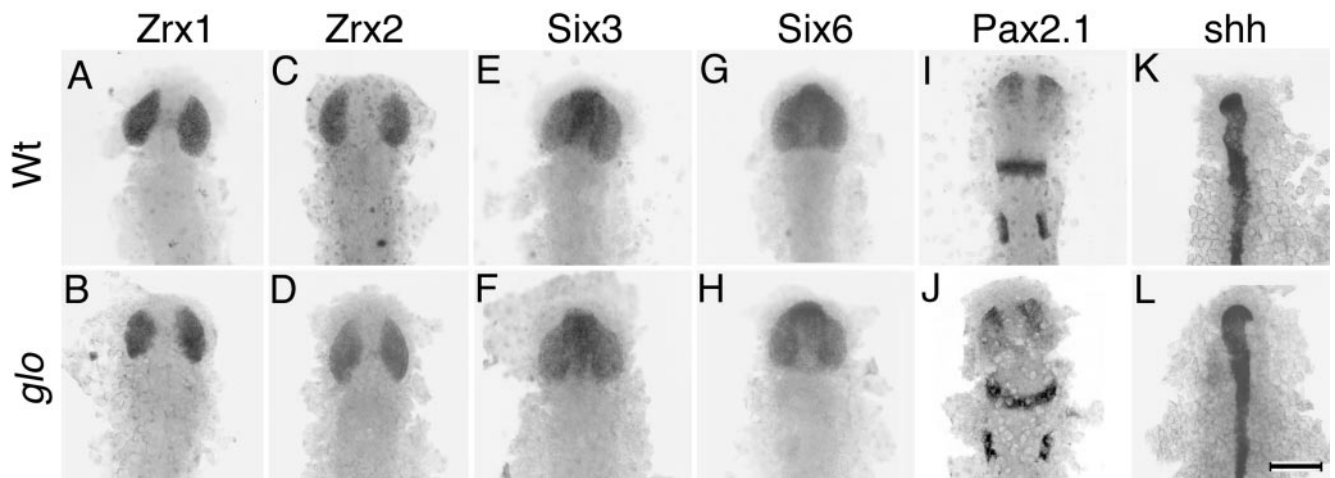


FIG. 7. Expression of early patterning genes in the anterior neural keel and optic primordia as revealed by *in situ* hybridization. No differences in expression patterns are detectable between wild-type (Wt) and mutant (*glo*) embryos. (A, B) *Zrx1*. (C, D) *Zrx2*. (E, F) *Six3*. (G, H) *Six6*. (I, J) *Pax2.1*. (K, L) *shh*. All panels show dorsal views of 12 hpf embryos with anterior to the top. Scale bar equals 100 μm .

with the ventricular surface both in the retina and in the brain (Figs. 8A, 8E, 8C, and 8G). The centrosomes of these cells are consistently located at the ventricular surface (Fig. 8, small green dots). No centrosomes were located more than one nuclear diameter from the ventricular surface in the retina (18 independent clones from 5 embryos) or in the brain (18 independent clones from 3 embryos). In these experiments, on rare occasions only, centrosomes appear to be somewhat removed from the apical surface. This usually correlates with the presence of an M-phase nucleus as indicated by anti-phosphorylated H3 histone staining (arrowhead in Fig. 8E inset and arrowhead in Fig. 8F). We have shown that, by 14.5 hpf, *glo* neuroepithelial cells display rounded morphology and do not align their apical termini at the ventricular surface (Figs. 3 and 4). If the *glo* phenotype is cell-autonomous, the same will be seen in mosaic animals and the centrosomes of the *glo* cells will be found away

from the ventricular surface. In contrast, if the *glo* neuroepithelial phenotype is cell-nonautonomous, the centrosomes of *glo* cells will align at the apical surface in the same way as in wild-type cells. Our experiments indicate that the latter is true. In the environment of wild-type epithelia, both in the brain (Fig. 8H) and in the eye (Fig. 8F), centrosomes of *glo* cells align at the ventricular surface. No centrosomes were located more than one nuclear diameter from the ventricular surface in the retina (13 independent clones from 3 embryos) or in the brain (7 independent clones from 2 embryos). These results indicate that the *glo* mutation acts cell-nonautonomously in the neuroepithelium of the retina and brain. The cell-nonautonomous behavior of the *glo* neuroepithelial phenotype reveals that cell-cell interactions play an important role in the maintenance of eye and brain neuroepithelial integrity in the early zebrafish embryo.

FIG. 6. Distribution of individual retinal cell classes in wild-type and mutant embryos. (A–F) Confocal laser scanning microscope images of transverse sections of wild-type (Wt) or mutant (*glo*) retinæ at 84 hpf. (A) Wild-type embryos exhibit a well-defined ganglion cell layer (arrows) and optic nerve (visualized with the Zn8 antibody and Cy3 fluorescence). (B) In *glo* embryos, on the other hand, ganglion cells form disorganized clusters (arrows) and the optic nerve is not detectable. Fascicles of ganglion cell neurites form in abnormal locations (arrowhead). (C) In wild-type embryos, processes of Muller glia, visualized with an anti-carbonic anhydrase antibody and Cy3 fluorescence, extend into the photoreceptor and ganglion cell layers. (D) In *glo* embryos, Muller glia lack processes and their cell bodies display a scattered distribution. (E) In the wild type, red-green double cones, here visualized with the Zpr-1 primary antibody and Alexa Fluor 488-conjugated secondary antibody, form a continuous cell layer (arrows). (F) In contrast, photoreceptor cells in mutant retinæ appear to be fewer in number and form rosettes (indicated with arrows). (G–L) Red-, blue-, and rod-opsin expressing photoreceptor cells revealed using *in situ* hybridization. (G) Red-opsin expressing cells in the wild-type outer nuclear layer are elongated and accumulate opsin mRNA mostly at the ventricular pole of the cell. (H) In mutant retinæ, red-opsin expressing cells form rosettes. The opsin-rich photoreceptor poles are directed toward the center of these rosettes. The same is true for blue-opsin expressing cells in wild-type (I) and mutant (J) retinæ, and rod-opsin expressing cells in the wild type (K) and the mutant (L). The elongated appearance of opsin expressing cells is partially preserved in mutant cells (H, J, L, compare with the wild type in G, I, K). *le*, lens. Scale bar equals 80 μm in (A–F) and 20 μm in (G–L).

DISCUSSION

We have found that during retinal neurogenesis in the zebrafish mutant *glass onion* (*glo*), individual cell classes are specified but do not localize to their normal positions. Prior to neurogenesis, neuroepithelia of mutant embryos lose the normal morphology and apical-basal polarity found in wild-type retinæ. This is not a general defect of epithelial development as the epidermis and parts of the spinal cord or even brain neuroepithelia are not affected. In the affected areas, markers which normally localize to the ventricular pole of neuroepithelial cells distribute ectopically, indicating that polarity is disrupted in *glo* neuroepithelial sheets. Genetic mosaic studies revealed that cell-cell interactions participate in the development of normal retinal neuroepithelial cell morphology shortly after the formation of the optic primordia.

***glass onion* Affects at Least Some Aspects of Neuroepithelial Cell Polarity**

Cells of both vertebrate and invertebrate epithelia display polarity characterized by asymmetric distribution of cellular organelles as well as the presence of two distinct cell surface regions: the apical and the basolateral plasma membrane domains. These two domains are separated by a belt of cell junctions and are characterized by the presence of specific protein constituents (Hinds and Ruffett, 1971; Bacallao *et al.*, 1989; Aaku-Saraste *et al.*, 1996; Chenn *et al.*, 1998). Genetic analysis in *Drosophila* revealed numerous genes which disrupt polarity and integrity in several epithelia. These phenotypes are characterized to a variable degree by a loss of one or more cell junction types, loss of cell morphology, and abnormal distribution of cell surface domain-specific components (reviewed in Muller, 2000). In addition, the cell proliferation rate is frequently increased in these mutant strains. Mutations of the *scribble* gene, for example, cause a loss of monolayer organization of embryonic epithelia, rounding of cell morphology, and the mislocalization of adherens junctions as well as apical proteins. Baso-lateral proteins, however, retain the normal distribution (Bilder and Perrimon, 2000). The *glass onion* phenotype displays characteristics that are reminiscent of fly mutants. The *glo* cells round up, do not maintain a characteristic polarized distribution of subcellular structures such as centrosomes and adherens junctions, and appear to proliferate at a higher rate. Despite these observations, it remains possible that apical and baso-lateral cell surface domains of the neuroepithelial cells are at least partially preserved in this mutant. Because markers of individual cell surface domains in the neuroepithelial sheet are not available, this possibility cannot be currently excluded.

***glass onion* Reveals Genetically Distinct Spatial and Temporal Subdivisions in Developing Neuroepithelium**

The possibility that neuroepithelial development is controlled by genetic pathways specific to particular developmental periods or particular spatial domains is supported by our analysis of the *glo* phenotype as well as a previously characterized mutant *ome* (Malicki and Driever, 1999). Although both the *glo* and *ome* mutations disrupt lamination in the retina, only the *glo* mutation affects both brain and eye neuroepithelia. *ome* appears to be specific to the retinal neuroepithelium. A more subtle spatial specificity is observed in *glo*. The loss of integrity in the *glo* neural tube does not affect the dorsal-most and some ventral-most regions of the brain neuroepithelium. Furthermore, the *glo* phenotype appears over 12 h before the onset of the *ome* phenotype (Malicki and Driever, 1999) but is absent at the very earliest stages of neural tube formation. These observations suggest the presence of genetically distinct temporal and spatial domains of development of the eye and brain neuroepithelia.

The presence of a neuroepithelial region in the dorsal-most neural tube which is unaffected by the *glo* phenotype may be explained in several ways. The most obvious possibility is that the *glo* gene may not be expressed in this region. It is also possible that the *glo* gene is active in these areas but may function in a pathway for which a redundant mechanism exists. This mechanism enables the wild-type phenotype of the neuroepithelium to be maintained in *glo* mutant embryos. Finally, it is possible that, in the dorsal-most region of the neuroepithelial sheet, cells express the *glo* gene at levels higher than that found elsewhere. All these mechanisms are consistent with the presence of spatial domains within the developing neuroepithelium which are under differential genetic control. To our knowledge, these domains do not correlate with any distinct morphological or histological features of neuroepithelial cells such as the shape of their apical or basal processes or nuclei.

Similarly, the onset of the *glo*, *ome*, and *nok* phenotypes at different time points after the formation of the eye and brain neuroepithelia suggests the presence of genetically distinct temporal subdivisions in the development of this tissue (Malicki and Driever, 1999; X. Wei and J.M., unpublished results). Although the neuroepithelium in *glo* embryos does initially form, its integrity is lost rapidly in the retina and brain. This suggests that *glo* activity is not involved in the initial formation of this tissue but rather in its maintenance. The *ome* phenotype, in turn, is expressed many hours after *glo*. Although by histological criteria, the eye and brain neuroepithelia do not change between the formation of the neural tube and the onset of neurogenesis, different onsets of *glo*, *nok*, and *ome* phenotypes suggest that the genetic controls of their integrity do change. These changes may be related to the variation of cell-cycle length in the retina prior to neurogenesis (Hu and Easter, 1999).

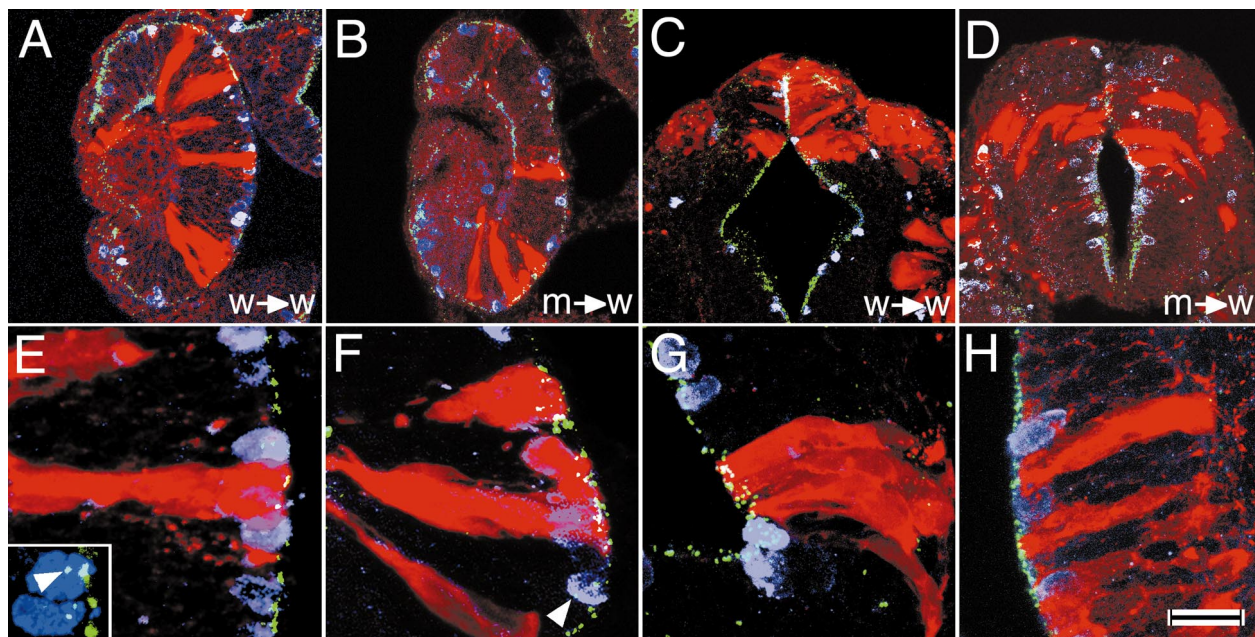


FIG. 8. Morphology of neuroepithelial cells and the location of their centrosomes and M-phase nuclei in mosaic embryos at ca. 24 hpf. Donor-derived cell clones are labeled with Alexa Fluor 488-conjugated avidin (red). The position of centrosomes is revealed using an anti- γ -tubulin primary antibody and a Cy5-conjugated secondary antibody (pseudocolored in green). The position of M-phase nuclei is revealed using an anti-phosphorylated H3 histone primary antibody and a Cy3-conjugated secondary antibody (pseudocolored in blue). Each image is a sum of multiple confocal sections collected along the z-axis. (A, E) In the wild-type environment of retinal neuroepithelium, the centrosomes of wild-type clones localize to the ventricular (apical) surface (18 out of 18 clones from 5 embryos). (C, G) Similar cell behavior is observed in the brain (18 out of 18 clones from 3 embryos). (B, F) In the environment of wild-type retina, the centrosomes of mutant cell clones also localize to wild-type positions (13 out of 13 clones in 3 embryos). (D, H) The same situation is observed in the brain (7 out of 7 clones in 2 embryos). In most cases, centrosomes which are located more than 1/2 nuclear diameter away from the ventricular surface are associated with M-phase nuclei (arrowhead in F and inset in E). Scale bar equals 30 μ m in (A–D); 9 μ m in (E–H).

They are not, however, related to any obvious histological transformations. Recent work has revealed a number of factors which regulate the early patterning of the optic primordia including members of the *Rx*, *Six*, *hedgehog*, and *Pax* families (Krauss *et al.*, 1993; Macdonald *et al.*, 1995; Lun and Brand, 1998; Nornes *et al.*, 1998; Seo *et al.*, 1998; Chuang *et al.*, 1999). By analyzing the expression of *Zrx1*, *Zrx2*, *Zrx3*, *Pax-2.1*, *Six-3*, *Six-6*, and *shh*, we found no evidence that the *glo* phenotype of the optic lobe neuroepithelium is caused by early patterning defects. Although we cannot exclude that yet other early patterning factors are affected in this mutant, these results suggest that the *glo* neuroepithelial defect is independent of the early patterning events.

The glass onion Neuroepithelial Defect Is Followed by Drastically Abnormal Neuronal Patterning

During early development, the retinal primordium consists of a single neuroepithelial cell layer. In *glo* mutants, these cells display loss of columnar shape and their apical termini cease to be aligned at the ventricular surface. Later, retinal cells become severely disorganized and many un-

dergo apoptotic cell death. Despite the severe abnormalities, individual neuronal cell types are specified in *glo* embryos but do not localize to their normal positions. How are the neuroepithelial and neuronal phenotypes related to each other? The *glo* mutation may mediate its effects via at least two mechanisms. First, it may act independently in these two aspects of retinal development. Alternatively, the early neuroepithelial defect could disrupt the subsequent neuronal patterning processes.

The possibility that the neuronal patterning defect arises from the abnormal development of the neuroepithelial cell layer is supported by the studies of retinal differentiation. Neurons are born at the ventricular surface of the retinal neuroepithelium and migrate to their appropriate locations to form well-defined cellular layers (Hinds and Hinds, 1974, 1979). The majority of, if not all, retinal cells are specified following the last mitotic division (Turner and Cepko, 1987; Holt *et al.*, 1988; Wetts and Fraser, 1988). Their migration and differentiation occur within the neuroepithelial sheet from which they are likely to take positional cues (Hinds and Hinds, 1974). The correct distribution of these cues, the nature of which remains unknown, may depend upon the preservation of apical–basal polarity in the neu-

roepithelial sheet. This reasoning supports the possibility that the *glo* mutation may disrupt retinal neurogenesis by preventing the correct distribution of positional cues in the neuroepithelial sheet.

Of all the cell classes assayed for in the retina, only interplexiform cells were undetectable in *glo* embryos at 84 hpf. In the wild-type zebrafish retina, they are first apparent at 60 hpf (Guo *et al.*, 1999). Their absence in *glo* embryos could be due to one of several possibilities. First, cells destined to differentiate into interplexiform cells may not have been specified from the progenitor pool of neuroepithelial cells. Second, cells fated to differentiate into interplexiform cells may have died prior to expressing detectable levels of tyrosine hydroxylase. Finally, interplexiform cells may have differentiated partially, so that, although this cell class is specified, it does not express late differentiation markers such as tyrosine hydroxylase. Previous studies have shown that cell–cell interactions are required for the elaboration of morphological and biochemical markers of cell-type identity (Hatta *et al.*, 1991; Halpern *et al.*, 1993; Stiemke *et al.*, 1994). The failure to form well-defined neuronal laminae could account for the inability of interplexiform cells to express tyrosine hydroxylase to detectable levels in *glo* embryos.

glass onion Reveals Cell–Cell Interactions in the Developing Retina

The neuroepithelial phenotype of the *glo* mutation is cell-nonautonomous at 24 hpf, indicating a defect in cell–cell interactions that take place prior to neurogenesis in the retina. When are these interactions likely to first take place? Using morphological and histological criteria, the *glo* phenotype is visible at 12 but not 10 hpf. This suggests that the cell–cell interactions, disrupted by the *glo* mutation, are present by ca. 12 hpf, shortly after the optic primordia have formed.

In wild-type embryos, the optic primordia are relatively simple lateral outpocketings of the neural keel. Which cells are involved in the neuroepithelial cell–cell interactions in the optic primordia? One or both of two types of intercellular interactions may be disrupted. The first possibility is that *glo* affects cell–cell interactions between neuroepithelial cells located next to each other within a single epithelial sheet. Such cell interactions have been characterized in other epithelia (reviewed in Drubin and Nelson, 1996). Alternatively, the *glo* mutation may disrupt signaling between cells located in different neuroepithelial sheets such as the ones which form the retinal primordium and the primordium of the retinal pigmented epithelium. The neuroepithelial cell layers which will ultimately form these structures are in close apposition and are likely to interact with each other (Schmitt and Dowling, 1994; Li *et al.*, 2000). An interaction between the neuroepithelial sheet and the retinal pigmented epithelium has recently been demonstrated in the mutant *mosaic eyes* (Jensen *et al.*, 2001).

What mechanisms are responsible for the rescue of the *glo* neuroepithelial phenotype in mosaic animals? A possible route through which cells may interact in mosaic animals is adherens junctions. Apart from a role in cell–cell adhesion, adherens junctions are presumed to function in signal transduction. They have been shown to contain molecules involved in cell–cell signaling such as cadherins, receptor tyrosine kinases, and *Notch* (reviewed in Bryant, 1997; Steinberg and McNutt, 1999; Muller, 2000). Signaling mediated by such molecular components could be disrupted in *glo*. Although the adherens junctions appear to be present both in *glo* and in the related mutant *ome*, their distribution is clearly abnormal. This is evidenced in these mutants by the abnormal distribution of actin foci. Electron microscopic analysis of *ome* has confirmed this observation (Malicki and Driever, 1999). Although the involvement of adherens junctions would suggest the presence of short-range signaling events possibly involving membrane-bound receptors and ligands, other mechanisms are also possible. These could involve extracellular matrix components deposited at the ventricular surface of the neuroepithelial sheet or diffusible signaling factors. Further studies will be necessary to reveal the nature of molecular events involved in cell–cell interactions revealed by the analysis of the *glass onion* phenotype.

ACKNOWLEDGMENTS

We thank Drs. Francesca Pignoni, Stephan Heller, Geoffrey Doerre, Xiangyun Wei, and Pascal Bang for comments on earlier versions of this manuscript. We are grateful to Peter Mathers and Deborah Stenkamp for providing us with Zrx cDNA clones and to John Dowling, Tom Vihtelic, and David Hyde for providing us with the zebrafish opsin probes. We are also thankful to Pavel Draber for the anti- γ -tubulin antibody and Paul Linsler for the anti-carbonic anhydrase antibody. Z.P. was supported by a Knights Templar Pediatric Ophthalmology Research Grant and J.M. by a Research to Prevent Blindness Career Development Award.

REFERENCES

- Aaku-Saraste, E., Hellwig, A., and Huttner, W. B. (1996). Loss of occludin and functional tight junctions, but not ZO-1, during neural tube closure–remodeling of the neuroepithelium prior to neurogenesis. *Dev. Biol.* **180**, 664–679.
- Aaku-Saraste, E., Oback, B., Hellwig, A., and Huttner, W. B. (1997). Neuroepithelial cells downregulate their plasma membrane polarity prior to neural tube closure and neurogenesis. *Mech. Dev.* **69**, 71–81.
- Abrams, J. M., White, K., Fessler, L. I., and Steller, H. (1993). Programmed cell death during Drosophila embryogenesis. *Development* **117**, 29–43.
- Andersen, S. S., and Bi, G. Q. (2000). Axon formation: A molecular model for the generation of neuronal polarity. *BioEssays* **22**, 172–179.
- Astrom, K. E., and Webster, H. D. (1991). The early development of the neopallial wall and area choroidea in fetal rats. A light and

- electron microscopic study. *Adv. Anat. Embryol. Cell Biol.* **123**, 1–76.
- Bacallao, R., Antony, C., Dotti, C., Karsenti, E., Stelzer, E. H., and Simons, K. (1989). The subcellular organization of Madin–Darby canine kidney cells during the formation of a polarized epithelium. *J. Cell Biol.* **109**, 2817–2832.
- Bilder, D., and Perrimon, N. (2000). Localization of apical epithelial determinants by the basolateral PDZ protein Scribble. *Nature* **403**, 676–680.
- Bryant, P. J. (1997). Junction genetics. *Dev. Genet.* **20**, 75–90.
- Cajal, S. R. (1893). La retina des vertebres. *La Cellule* **9**, 17–257.
- Chenn, A., Zhang, Y. A., Chang, B. T., and McConnell, S. K. (1998). Intrinsic polarity of mammalian neuroepithelial cells. *Mol. Cell. Neurosci.* **11**, 183–193.
- Chuang, J. C., Mathers, P. H., and Raymond, P. A. (1999). Expression of three Rx homeobox genes in embryonic and adult zebrafish. *Mech. Dev.* **84**, 195–198.
- Dowling, J. (1987). “The Retina.” Harvard Univ. Press, Cambridge, MA.
- Drubin, D. G., and Nelson, W. J. (1996). Origins of cell polarity. *Cell* **84**, 335–344.
- Easter, S., and Nicola, G. (1996). The development of vision in the zebrafish (*Danio rerio*). *Dev. Biol.* **180**, 646–663.
- Gavrieli, Y., Sherman, Y., and Ben-Sasson, S. (1992). Identification of programmed cell death in situ via specific labeling of nuclear DNA fragmentation. *J. Cell Biol.* **119**, 493–501.
- Geiger, B., Schmid, E., and Franke, W. W. (1983). Spatial distribution of proteins specific for desmosomes and adherens junctions in epithelial cells demonstrated by double immunofluorescence microscopy. *Differentiation* **23**, 189–205.
- Georges-Labouesse, E., Mark, M., Messaddeq, N., and Gansmuller, A. (1998). Essential role of $\alpha 6$ integrins in cortical and retinal lamination. *Curr. Biol.* **8**, 983–986.
- Guo, S., Wilson, S. W., Cooke, S., Chitnis, A. B., Driever, W., and Rosenthal, A. (1999). Mutations in the zebrafish unmask shared regulatory pathways controlling the development of catecholaminergic neurons. *Dev. Biol.* **208**, 473–487.
- Haffter, P., Granato, M., Brand, M., Mullins, M. C., Hamerschmidt, M., Kane, D. A., Odenthal, J., van Eeden, F. J., Jiang, Y. J., Heisenberg, C. P., Kelsh, R. N., Furutani-Seiki, M., Vogel-sang, E., Beuchle, D., Schach, U., Fabian, C., and Nusslein-Volhard, C. (1996). The identification of genes with unique and essential functions in the development of the zebrafish, *Danio rerio*. *Development* **123**, 1–36.
- Halpern, M., Ho, R., Walker, C., and Kimmel, C. (1993). Induction of muscle pioneers and floor plate is distinguished by the zebrafish no tail mutation. *Cell* **75**, 99–111.
- Hatta, K., Kimmel, C., Ho, R., and Walker, C. (1991). The cyclops mutation blocks specification of the floor plate of the zebrafish central nervous system. *Nature* **350**, 339–341.
- Hendzel, J. M., Wei, Y., Mancini, M. A., Van Hooser, A., Ranalli, T., Brinkley, B. R., Bazett-Jones, D. P., and Allis, C. D. (1997). Mitosis-specific phosphorylation of histone H3 initiates primarily within pericentromeric heterochromatin during G_2 and spreads in an ordered fashion coincident with mitotic chromosome condensation. *Chromosoma* **106**, 348–360.
- Hinds, J., and Hinds, P. (1974). Early ganglion cell differentiation in the mouse retina: an electron microscopic analysis utilizing serial sections. *Dev. Biol.* **37**, 381–416.
- Hinds, J., and Hinds, P. (1979). Differentiation of photoreceptors and horizontal cells in the embryonic mouse retina: An electron microscopic, serial section analysis. *J. Comp. Neurol.* **187**, 495–512.
- Hinds, J. W., and Ruffett, T. L. (1971). Cell proliferation in the neural tube: an electron microscopic and golgi analysis in the mouse cerebral vesicle. *Z. Zellforsch. Mikrosk. Anat.* **115**, 226–264.
- Ho, R. K., and Kane, D. A. (1990). Cell-autonomous action of zebrafish spt-1 mutation in specific mesodermal precursors. *Nature* **348**, 728–730.
- Holt, C., Bertsch, T., Ellis, H., and Harris, W. (1988). Cellular determination in the *Xenopus* retina is independent of lineage and birth date. *Neuron* **1**, 15–26.
- Hu, M., and Easter, S. S. (1999). Retinal neurogenesis: The formation of the initial central patch of postmitotic cells. *Dev. Biol.* **207**, 309–321.
- Humphrey, C., and Pittman, F. (1974). A simple methylene blue-azure II-basic fuchsin stain for epoxy-embedded tissue sections. *Stain Technol.* **49**, 9–14.
- Jensen, A. M., Walker, C., and Westerfield, M. (2001). *mosaic eyes*: A zebrafish gene required in pigmented epithelium for apical localization of retinal cell division and lamination. *Development* **128**, 95–105.
- Kimmel, C. B., Ballard, W. W., Kimmel, S. R., Ullmann, B., and Schilling, T. F. (1995). Stages of embryonic development of the zebrafish. *Dev. Dyn.* **203**, 253–310.
- Krauss, S., Concordet, J. P., and Ingham, P. W. (1993). A functionally conserved homolog of the *Drosophila* segment polarity gene *hh* is expressed in tissues with polarizing activity in zebrafish embryos. *Cell* **75**, 1431–1444.
- Li, Z., Joseph, N. M., and Easter, S. S. (2000). The morphogenesis of the zebrafish eye, including a fate map of the optic vesicle. *Dev. Dyn.* **218**, 175–188.
- Lun, K., and Brand, M. (1998). A series of no isthmus (*noi*) alleles of the zebrafish *pax2.1* gene reveals multiple signaling events in development of the midbrain-hindbrain boundary. *Development* **125**, 3049–3062.
- Macdonald, R., Barth, K. A., Xu, Q., Holder, N., Mikkola, I., and Wilson, S. W. (1995). Midline signaling is required for Pax gene regulation and patterning of the eyes. *Development* **121**, 3267–3278.
- Malicki, J. (1999). Development of the retina. *Methods Cell Biol.* **59**, 273–299.
- Malicki, J., and Driever, W. (1999). *oko meduzy* mutations affect neuronal patterning in the zebrafish retina and reveal cell–cell interactions of the retinal neuroepithelial sheet. *Development* **126**, 1235–1246.
- Malicki, J., Neuhauss, S. C., Schier, A. F., Solnica-Krezel, L., Stemple, D. L., Stainier, D. Y., Abdelilah, S., Zwartkruis, F., Rangini, Z., and Driever, W. (1996). Mutations affecting development of the zebrafish retina. *Development* **123**, 263–273.
- Muller, H. A. (2000). Genetic control of epithelial cell polarity: Lessons from *Drosophila*. *Dev. Dyn.* **218**, 52–67.
- Muller, H. A., and Wieschaus, E. (1996). *armadillo*, *bazooka*, and *stardust* are critical for early stages in formation of the zonula adherens and maintenance of the polarized blastoderm epithelium in *Drosophila*. *J. Cell Biol.* **134**, 149–163.
- Nawrocki, W. (1985). “Development of the Neural Retina in the Zebrafish, *Brachydanio rerio*.” University of Oregon, Eugene, OR.
- Nornes, S., Clarkson, M., Mikkola, I., Pedersen, M., Bardsley, A., Martinez, J. P., Krauss, S., and Johansen, T. (1998). Zebrafish

- contains two pax6 genes involved in eye development. *Mech. Dev.* **77**, 185–196.
- Oppenheim, R. W. (1985). Naturally occurring cell death during neural development. *Trends Neurosci.* **8**, 487–493.
- Oxtoby, E., and Jowett, T. (1993). Cloning of the zebrafish krox-20 gene (*krx-20*) and its expression during hindbrain development. *Nucleic Acids Res.* **21**, 1087–1095.
- Rodieck, R. W. (1973). "The Vertebrate Retina: Principles of Structure and Function." W. H. Freeman & Co., San Francisco, CA.
- Sauer, F. C. (1935). Mitosis in the neural tube. *J. Comp. Neurol.* **62**, 377–405.
- Schmitt, E., and Dowling, J. (1994). Early eye morphogenesis in the Zebrafish *Brachydanio rerio*. *J. Comp. Neurol.* **344**, 532–542.
- Seo, H. C., Drivenes, Ellingsen, S., and Fjose, A. (1998). Expression of two zebrafish homologues of the murine Six3 gene demarcates the initial eye primordia. *Mech. Dev.* **73**, 45–57.
- Steinberg, M. S., and McNutt, P. M. (1999). Cadherins and their connections: Adhesion junctions have broader functions. *Curr. Opin. Cell Biol.* **11**, 554–560.
- Stearns, T., and Kirschner, M. (1994). In vitro reconstitution of centrosome assembly and function: The central role of γ -tubulin. *Cell* **76**, 623–637.
- Stiemke, M. M., Landers, R. A., Al-Ubaidi, M. R., Rayborn, M. E., and Hollyfield, J. G. (1994). Photoreceptor outer segment development in *Xenopus laevis*: Influence of the pigment epithelium. *Dev. Biol.* **162**, 169–180.
- Stumpo, D., Bock, C., Tuttle, J., and Blackshear, P. (1995). MARCKS deficiency in mice leads to abnormal brain development and perinatal death. *Proc. Natl. Acad. Sci. USA* **92**, 944–948.
- Tomasiewicz, H., Ono, K., Yee, D., Thompson, C., Goridis, C., Rutishauser, U., and Magnuson, T. (1993). Genetic deletion of a neural cell adhesion molecule variant (N-CAM-180) produces distinct defects in the central nervous system. *Neuron* **11**, 1163–1174.
- Tomita, K., Ishibashi, M., Nakahara, K., Ang, S. L., Nakanishi, S., Guillemot, F., and Kageyama, R. (1996). Mammalian hairy and Enhancer of split homolog 1 regulates differentiation of retinal neurons and is essential for eye morphogenesis. *Neuron* **16**, 723–734.
- Turner, D., and Cepko, C. (1987). A common progenitor for neurons and glia persists in rat retina late in development. *Nature* **328**, 131–136.
- Volberg, T., Geiger, B., Kartenbeck, J., and Franke, W. W. (1986). Changes in membrane-microfilament interaction in intercellular adherens junctions upon removal of extracellular Ca^{2+} ions. *J. Cell Biol.* **102**, 1832–1842.
- Westerfield, M. (1994). "The Zebrafish Book." University of Oregon Press, Eugene, OR.
- Wetts, R., and Fraser, S. (1988). Multipotent precursors can give rise to all major cell types of the frog retina. *Science* **239**, 1142–1145.

Submitted for publication November 15, 2000

Revised February 22, 2001

Accepted February 26, 2001

Published online May 1, 2001